Energy resolution analysis for the ILC luminometer

Jonathan Aguilar

1 ILC physics

1.1 International Linear Collider

The proposed International Linear Collider (ILC) will be an e^+e^- collider with a center-of-mass energy $\sqrt{s}$ of 500 GeV, with the option to upgrade to 1 TeV [7]. It represents the continuation of a global physics program dedicated to answering fundamental questions about the universe, and in particular, shedding further light on the investigations of the Large Hadron Collider. If the Higgs particle is found, it should be associated with very new physical phenomena that will be accessible to the ILC's energy range: namely, supersymmetry, extra dimensions of space, and even the existence of new forces. The ILC is expected to provide important tests of the results of the Large Hadron Collider in probing physics beyond the Standard Model. An e^+e^- collider is a powerful tool for precision measurements of particle masses and unambiguous particle spin determination [7].

The total luminosity required is $500 fb^{-1}$ during the first four years of operation, and double that during the first phase of operation at 500 GeV. It will have a peak luminosity of $2 \cdot 10^{34} cm^{-2} s^{-1}$

A great advantage of the ILC is its versatility and the possibility to upgrade after several years of running, if this is required by new physics discovered. It will be capable of operating in GigaZ mode, where it runs on the Z-resonance with high luminosity and with both beams polarized, producing 10^9 hadronic Z decays in less than a year [7]. Secondly, the ILC could also run at the W-pair production threshold for high-precision measurement of the W-mass. Thirdly, both accelerators could accelerate electrons for an e^-e^- collider instead of an e^+e^-. This would help determine the mass of the super-symmetric selectron particle, if it exists within the ILC energy range. Finally, by colliding electrons with a photon beam, the ILC could produce a high energy, high quality photon beam ($e^-\gamma$ or $\gamma\gamma$) collider.

1.2 International Large Detector

The International Large Detector (ILD) concept is a proposed to be a multi-purpose detector which provides excellent precision in spatial and energy resolution over a large solid angle. In particular, this required to achieve the goal of particle track reconstruction

The ILD is one of three detector designs validated by the International Detector Advisory Group in August of 2009 [2].

2 Luminosity Measurement

LumiCal is the luminometer of the ILD, designed to measure the integrated luminosity of the ILC beam. From the physics program, relative precision in the luminosity measurement of better that 10^{-3} is required. Small angle Bhabha scattering will be used for this measurement [6].

The integrated luminosity is estimated by counting the number of Bhabha events using the well-known Bhabha scattering cross-section, according to the relation $N_{Bh} = \mathcal{L} \cdot \sigma_{Bh}$, so

$$\mathcal{L} = \frac{N_{Bh}}{\sigma_{Bh}}. \tag{1}$$

N_{Bh} must be measured with sufficient precision that $\frac{\Delta \mathcal{L}}{\mathcal{L}} \leq 10^{-3}$.

2.1 Relative error in luminosity

There are several terms that contribute to the relative error in luminosity:

$$\frac{\Delta \mathcal{L}}{\mathcal{L}} = \frac{\Delta \mathcal{L}}{\mathcal{L}}_{stat} \oplus \frac{\Delta \mathcal{L}}{\mathcal{L}}_{sys} \oplus \frac{\Delta \mathcal{L}}{\mathcal{L}}_{other} \tag{2}$$

The statistical contribution is proportional to the variance in the number obsevered Bhabha scatterings, N. This is Poisson distributed:

$$\frac{\Delta \mathcal{L}}{\mathcal{L}} = \frac{\Delta N}{N} = \frac{\sqrt{N}}{N} = \frac{1}{\sqrt{N}}. \tag{3}$$

Therefore, if $O(10^6)$ Bhabha events will be counted, the required precision in luminosity is $1/\sqrt{10^6} = 10^{-3}$

The fundamental source of error in luminosity comes from miscounting of Bhabha events:

$$\frac{\Delta \mathcal{L}}{\mathcal{L}} = \frac{\Delta N}{N} = \frac{N_{real} - N_{count}}{N_{real}} \tag{4}$$

Counting accuracy is limited by factors such as energy resolution and position reconstruction.

The Bhabha scattering cross-section has a very strong dependence on polar angle [14]:

$$\frac{d\sigma}{d\theta} \propto \frac{1}{\theta^3},$$

(5)

making the inner radius of LumiCal perhaps the most important parameter in its construction. It is important to make the inner radius low enough to gather sufficient statistics for luminosity determination, but so low that the background is overwhelming. For some distance d from the interaction point of the ILC, the dependence of $\Delta\mathcal{L}/\mathcal{L}$ on the angle θ_{min} between the beam and the inner radius is given by:

$$\frac{\Delta\mathcal{L}}{\mathcal{L}} = 2\frac{\Delta r_{cluster}}{r_{clus}} \approx 2\frac{\Delta r_{clus}}{d\,\theta_{min}},$$

(6)

where r_{clus} is the radial position of clusters detected in the calorimeter, Δr_{clus} is its uncertainy, and in the small angle approximation, $\theta_{min} \approx r_{clus}/d$. Because of this strong dependence on polar angle, it is necessary to know the position of the inner radius to within $4\,\mu m$ [5].

Physics requirements put important limits on the construction of LumiCal. The necessary precision in position reconstruction, especially because of the sensitivity of the Bhabha cross-section to the inner radius means that the position of LumiCal must be known to a few hundred microns [10].
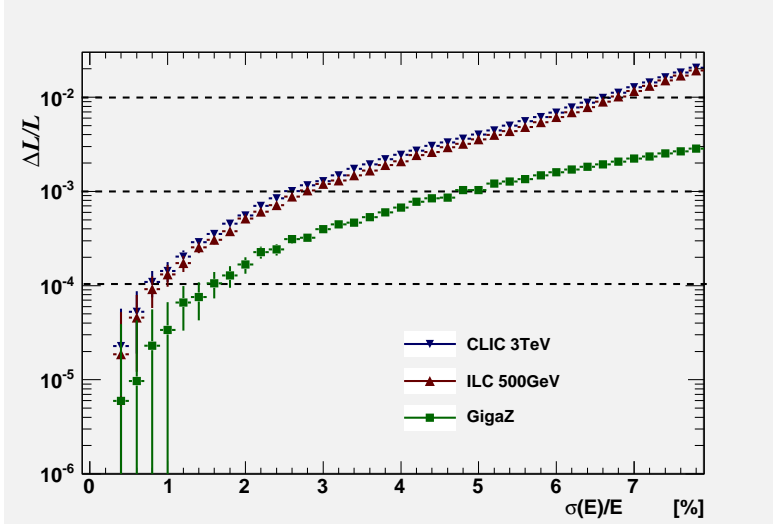

Figure 1: Luminosity error dependence on energy resolution. The goal is better than 10^{-3}.

Most relevant to this paper, describe the dependence of $\frac{\Delta\mathcal{L}}{\mathcal{L}}$ on σ_E/E here.

3   Work scope

The design parameters of LumiCal have been the the subject of much previous attention, and are discussed in section 4. The purpose of this work has been to use Monte Carlo simulation techniques to characterize the energy resolution of the LumiCal design and examine its effect on the luminosity measurement.

4   LumiCal design

4.1   Constraints and considerations

Equation 4 makes it clear that accurately counting Bhabha events is critically important in determining the error in relative luminosity. Bhabha events must be correctly identified from the background, placing demands on particle energy and position reconstruction. These are the main contributors to error in relative luminosity, and LumiCal must be designed to take this into account. Accurately determining the energy of incident particles requires that not only should as much of the shower energy as possible should be contained within the detector volume, but also that a sufficient fraction of the energy be deposited within sensors.

Event selection also depends on position reconstruction, and does so in two ways. First, because of irregularities in the geometry of LumiCal, energy deposition is dependent on azimuthal angle and therefore energy reconstruction also depends on the accuracy of position reconstruction. Secondly, particle tracks from Bhabha scattering must be colinear in the two LumiCal modules to within a certain amount of error to be counted. The geometry optimization and justifications are expressed clearly in [13], and will be summarized where appropriate.

4.2   Current design

The mechanical design of LumiCal is described in [9, 11]. It will consist of two identical calorimeters, located symmetrically on opposite sides of the interaction point, 2.5 m away. Each calorimeter is designed as a hollow cylinder, divided into two halves so that it can be fitted around the beam pipe 2. For the rest of this section, the discussion will refer to a single calorimeter module of LumiCal, since the two calorimeters are identical.

4.2.1   Overview

LumiCal uses a highly modular design. Each calorimeter consists of 30 rings. Each ring is made of a 3.5 mm-thick layer of tungsten that acts as an absorber,
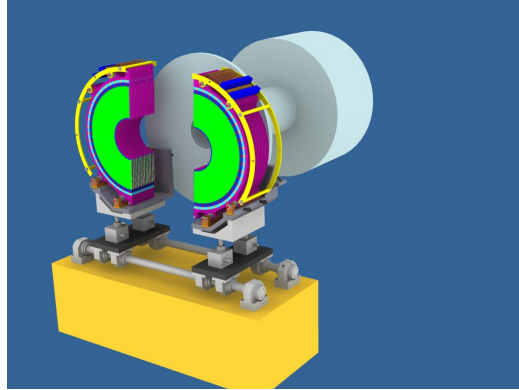
Figure 2: Closing LumiCal on the beam pipe with a temporary support [9]

and a 320 *µm*-thick silicon layer that serves as the sensor. The silicon is divided azimuthally into 12 tiles, and each tile is divided further into 4 sectors for a total of 48 azimuthal divisions. The angular width of each sector is 7.5°. Finally, each sector is divided radially into 64 Si pads with 1.8 mm pitch. Each pad has its own readout electronics. A single ring therefore has 3,072 pads, and there are a total of 92,160 pads in the entire detector.

There is a mechanical gap of 0.1 mm between adjacent tiles, and a further 1.2 mm of uninstrumented silicon on each tile edge which is occupied by guard rings. The width of this gap does not vary with radius and extends through the full length of the sensitive region, from 80 mm to 195.2 mm.

4.2.2   Inner and outer radii

The dimension of the inner radius is primarily determined by the θ^{-3} dependence of the Bhabha scattering cross-section (equation 5). It is important to place the calorimeter as close to the beam as possible to increase the statistical power of the measurement; however, it has been shown that at distances below 70 mm, backscattering of beamstrahlung electrons becomes significant and increases the noise in LumiCal and in surrounding experiments. The mechanical inner radius was therefore set at 76 mm, which was found to be a good compromise [13]). The sensitive inner radius is offset by 4 mm to 80 mm from the beam. The outer radius is set by the number and pitch of the sensitive Si pads - $80 + 64 \cdot 1.8 = 195.2$ mm. This gives LumiCal an angular coverage of 32 mrad - 78 mrad. The fiducial volume, in which 95% of the shower energy is contained, is between about 40 and 69 mrad.

The mechanical outer radius was set at 224.5 mm for these simulations, but is currently under debate and ultimately will depend on the design of the readout
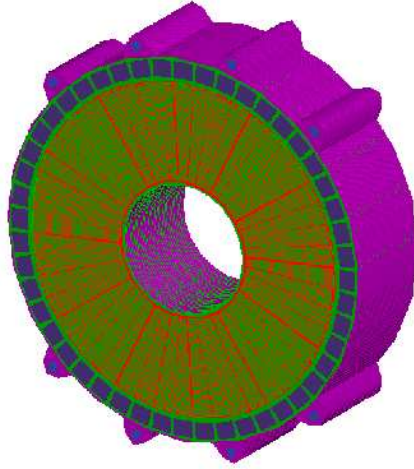
Figure 3: One of two identical LumiCal calorimeters

electronics. However, because Bhabha scattering falls off quickly, this parameter is of less importance to the overall luminosity measurement.

4.2.3 Number of layers

In order to contain the shower, a total number of 30 radiation lengths is required. Thinner layers give better energy resolution but are more expensive due to the increased amount of instrumentation required. 30 rings with 3.5 mm-thick absorbers was found to give sufficiently good energy resolution. In two simulations of calorimeter designs consisting of 50 layers and 90 layers, it was determined that no improvement in position resolution is seen after the 30th layer [8, 13]. The absorber is one radiation-length ($X_0 = 3.5mm$) thick, and the Si sensors are $320\mu m$ thick. The silicon tile is glued to a thin kapton foil for electrical insulation, and then placed directly on the tungsten. Current specifications state that there will be 0.92 mm of space between tungsten absorbers, into which must fit the Si sensors and readout electronics. Since the tile gaps are not instrumented, alternating layers will be rotated by $3.75°$ to reduce energy loss in the tiles.

4.2.4 Radial and azimuthal divisions

Requirements for the number of radial and azimuthal divisions are determined solely by requirements in position reconstruction, not energy resolution, and again are discussed in [13]. Radial sensor cell size affects the polar angle reconstruction resolution and bias. Both of these values decrease as the cell size decreases. With

a constant pitch of 1.8 mm, the angular cell size varies between 0.7156 and 0.7189 mrad over the sensitive area. However, as cell size decreases, cross-talk between electronics increases. This places a limit on the radial cell dimension, and 1.8 mm (64 cells) was found to be a good compromise. The contribution this makes to the total relative luminosity error is on the order of 10^{-4}. Similarly, 48 azimuthal divisions was found to give the best compromise between azimuthal angle resolution and electronic noise. This contribution to relative luminosity error is predicted to be on the order of 10^{-5}.

5   Simulation

5.1   Software used

The LumiCal simulation was constructed using Geant4.9.1 [1], a C++ object-oriented toolkit for simulating the interaction of particles and matter. Geant4 makes it possible to describe complex geometries and materials, as well as energetic particles and their various modes of interaction and decay. It also took advantage of the ILD detector software

Unique about the simulation is that it was designed to be independent of Mokka [4], the Geant4-based software framework used to maintain standards and compatibility among the different detectors of the ILC. The main advantage was that this model allows us to define our own magnetic field in such a way that the value does not need to be checked each time a particle steps. This provides a slight improvement in simulation speed.

5.2   Simulated Geometry

The simulated model for LumiCal was constructed to reproduce as accurately as possible the actual geometry, as described in Section 4. Table 1 shows the geometrical parameters of the simulated calorimeter:

The electronics were modeled as a solid layer consisting of a blend of kapton, copper, and epoxy in the proportions specified in [9].

An image of the tile gap as implemented in the simulation is shown in figure 4.

5.3   Simulation procedure

To estimate energy resolution, one calorimeter module was bombarded with monoenergetic single electrons at 50 GeV, 100 GeV, 150 GeV, 200 GeV, 250 GeV,

LumiCal simulation parameters			
Number of radial cells	:	64	
Number of sectors	:	48	
Number of planes	:	30	
Length	:	132.4	[mm]
Distance from IP	:	2502.6	[mm]
Inner radius	:	76.0	[mm]
Outer radius	:	224.5	[mm]
Sensor inner radius	:	80.0	[mm]
Sensor outer radius	:	195.2	[mm]
Cell radial pitch	:	1.762	[mm]
Sector width	:	7.5	[deg]
Gap between absorber plates	:	0.915	[mm]
Air gap	:	0.200	[mm]
Tile gap (2x per tile)	:	1.200	[mm]
Layer ϕ offset	:	3.750	[deg]
Front-end chip thickness	:	1.000	[mm]
Front fanout thickness	:	0.160	[mm]
Back fanout thickness	:	0.235	[mm]
Si sensor thickness	:	0.320	[mm]
Tungsten thickness	:	3.500	[mm]
Total plane thickness	:	4.415	[mm]
Mass of LumiCal (1 module)	:	280.972	[kg]

LumiCal polar angle (θ) acceptance [rad]			
		geometrical	fiducial
Detector θ_{min}	:	0.031	0.033
Detector θ_{max}	:	0.077	0.073
Front-end θ_{min}	:	0.075	
Front-end θ_{max}	:	0.089	

Table 1: List of geometric parameters used in the simulation, and the resulting polar angles.
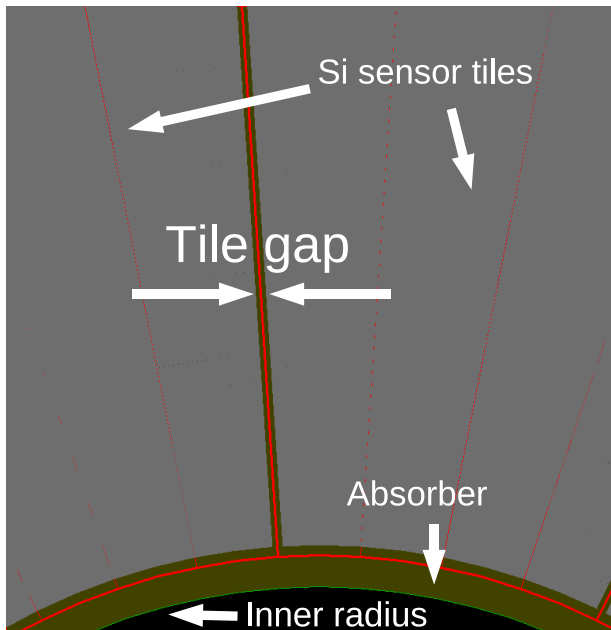
Figure 4: Image of the tile gap taken from the LumiCal simulation

and 300 GeV. 1000 primary electrons were generated per energy and were randomly distributed across the entire volume of LumiCal. The LHEP physics list [3] was used to determine interactions.

Electrons inside the detector interact with the detector material, showering and depositing energy according the physics list. If the energy deposition occured inside a silicon sensor volume, the energy was recorded.

When an electron's track intersected with the first plane of the detector, Geant4 would step through interactions with the calorimeter material and deposit energy until it reached the range cut-off of 5 μm. This meant that the particle had lost sufficient energy that over the next step, it would travel less than 5 μm in the medium. At this point, the particle was stopped by Geant4 and all remaining energy was deposited into the current volume. The beam crossing angle was aligned with the central axis of LumiCal. The magnetic field was 3.5 T everywhere.

6 Results

6.1 Determining Energy Resolution

LumiCal measures the total energy deposited in the calorimeter in order to estimate the number of Bhabha pairs generated by the ILC beam. The energy resolution determines the size of the error on the number of pairs, which determines the error on luminosuty $\mathcal{L}$ as given in equation 1.

The model used to describe energy resolution is given as

$$\frac{\sigma_E}{E} = \sqrt{\left(\frac{a}{\sqrt{E}}\right)^2 + b^2} \tag{7}$$

where E is the energy of the incident particle. The constant *a* corresponds to statistical fluctuations and imposes a fundamental limit from physics on the energy resolution of the calorimeter, for a given design. The second term, *b*, corresponds to leakage – when particles do not deposit all their energy in the detector. Generally this is associated with particles that are incident on the edges of the detector: Particles at very high or very low azimuthal angles (< 40 mrad or > 69 mrad, the angles which define the fiducial volume) will contribute to leakage because they will simply not pass through enough of the detector to deposit all their energy. There is little that can be done about this besides extending the size of the calorimeter (this too can be problematic, though, due to the increased beam background at low values of θ). However, even for particles that are incident *within* the fiducial volume, the tile gaps add an uninstrumented region in which energy deposition is not recorded, and presumably impact energy resolution. This effect had not previously been investigated by the FCAL collaboration.

The physical interpretation of energy resolution is extracted from the value of the constants, *a* and *b* (sometimes there are more terms with corresponding constants, but those did not apply to this simulation) [12]. To determine σ_E/E, the calorimeter is bombarded with particles at various energies, with large numbers of particles at each energy. The rms of energy deposition for particles of a given energy is calculated and divided by the initial particle energy. Then this value is plotted against inital particle energy, and equation 7 is fitted to the data.

6.2 Effect of tile gaps on energy resolution

As previously described, the layers of LumiCal are rotated by $3.75°$, or half a sector, in order to reduce the effects of energy loss from electrons that hit the uninstrumented gaps between tiles. It is important then to characterize the reduction in energy deposition caused by the tile gaps. Figure 5(a) shows electron

energy deposition plotted against azimuthal angle, for a monoenergetic beam of 250 GeV electrons randomly distributed in ϕ and θ across the entire volume. The most striking feature is the large decreases in energy deposition that correspond precisely to the location of the tile gaps - both the $30°$ spaces between tiles as well as the $3.75°$ rotation between subsequent layers are clearly resolved. In the worst case, tile gap electrons only deposit about 80% of the average deposited energy per particle. Furthermore, a significant portion of the electrons - about 18%, are incident on or near the tile gaps.

To better understand the effect of the tile gaps on energy resolution, the data from the MC simulation were separated into four sets. The first included all the particles incident on the calorimeter. The other three included increasingly large cuts to the data based on the azimuthal angle of the primary particle. The least inclusive cut ignored energy deposited by any primary particle directly incident on a tile gap (on layers of either rotation) – this was called the "gap-only" cut. The second cut ignored all primary particles incident on either the tile gaps or the $3.75°$ between – the "rotation-angle" cut. The third, and most inclusive, cut ignored all primary particles incident on the sectors directly adjacent to the tile gaps – the "sector" cut. Figures 5(b) – 5(d) are graphical representations of these cuts. Particles removed from the data set are colored red; particles that remained are colored blue.

% lost per cut	
Gap-only	18%
Rotation-angle	21%
Sector	62%

Table 2: % particles filtered out by the azimuthal angle cuts in figure 5.

These cuts reveal several interesting trends. The gap-only cut does not remove the set of particles in between gaps which have a lower average energy deposition than the particles incident on the center of the sensors, and which should therefore adversely impact energy resolution. However, figure 6 does not support this notion. In this figure, the energy resolution from each cut is plotted against primary particle energy. Firstly, all cuts show an improvement in energy resolution compared to including all particles. However, excluding more particles beyond the gap-only cut does not appear to make much of a difference, especially at high energies. It seems that particles incident between the tile gaps are not significant contributors to poorer energy resolution. Secondly, and perhaps most interestingly, the major improvement comes from the "second" term in the equation used to model energy resolution (eq. 7). As previously discussed, this term is associated with energy-independent losses in the calorimeter, and can be caused by
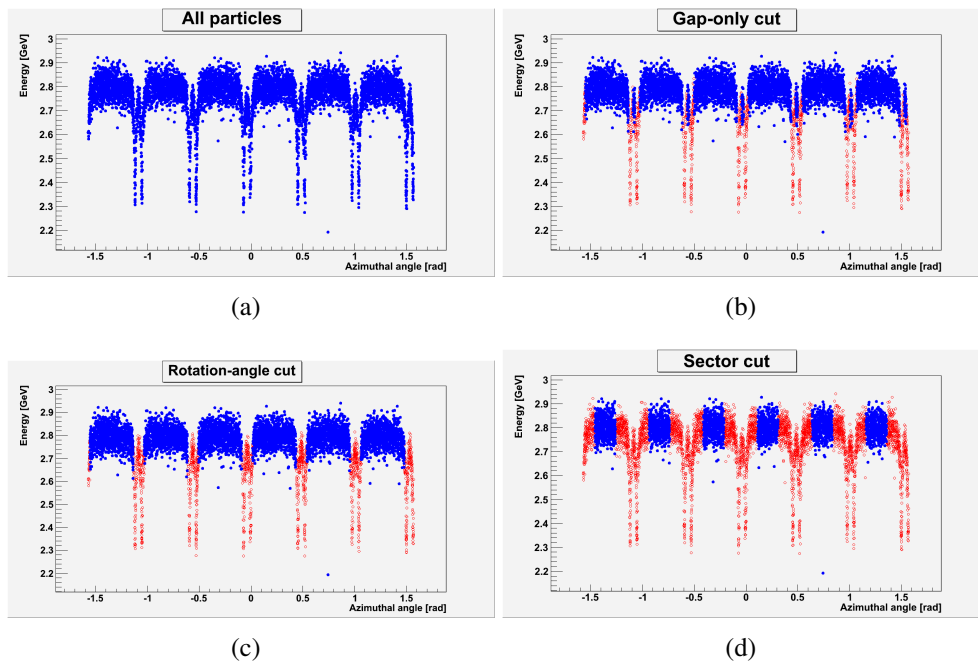
11

(a)	(b)
(c)	(d)

Figure 5: Energy deposition per 250 GeV electron vs. azimuthal angle ϕ. Note the well-defined tile gap regions of low energy deposition. The plots show: (a) all particles; (b) gap-only cut – only primary particles that actually hit a tile gap; (c) rotation-angle cut – covers the gaps and the angle of rotation between them; and (d) sector cut - sectors adjacent to tile gaps. Cut primaries indicated by hollow circles with red outline, and good primaries are indicated by solid blue circles. 12,000 particles were used to generate this sample.

irregularities in detector geometry. As can be seen in equation 7 and as explain in [12], these constant effects become more significant at higher energies. In figure 6, the energy resolution tends to converge at low energies and diverge at high energies. The solid lines show fits with equation 7, and the dashed line shows a fit to the full data set using $b = 0$, that is, ignoring the geometrical contribution. It is clear that in order to correctly model energy resolution, especially at high energies, the contribution from the tile gap must be considered.
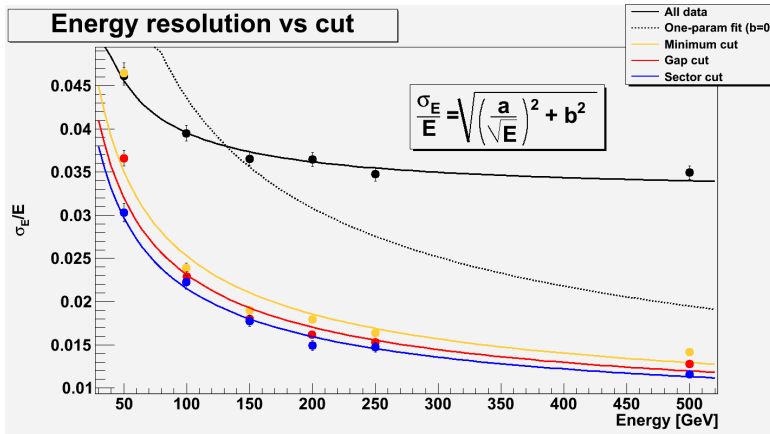

Figure 6: The greatest improvement comes from the narrowest cut over the tile gaps, further cuts only increase energy resolution slightly.

This is supported by figure 7, which show how the parameters of energy resolution vary as more and more electrons are excluded. As previously mentioned, a is usually associated with statistical fluctuations in the shower and b is associated with geometry-dependent loss due to particles leaking out of the detector or energy not being recorded due to some other geometrical effect. Here it is shown that a varies only by about 8% from the mean, with no clear relationship between its value and size of the cut. b, however, shows a distinct drop by a factor of 4 when all the data are included versus when the tile gaps have been excluded. Between the b values corresponding to tile gap cuts, however, the value changes by only about $\pm 3\%$ from the mean. In this case, it can be clearly seen that the improvement in energy resolution is almost entirely due to change in b, not in a. The leakage is presumably due to energy being deposited in the uninstrumented tile gaps, and therefore not being recorded.

Figure 8 confirms the important effect that the uninstrumented tile gaps have on energy resolution. It shows the energy resolution for two models of LumiCal, one with tile gaps implemented as in the mechanical design specifications, and the other without tile gaps - that is, an ideal LumiCal in which the sensor pads of the outside sectors on each tile meet, with no dead space in between. Both
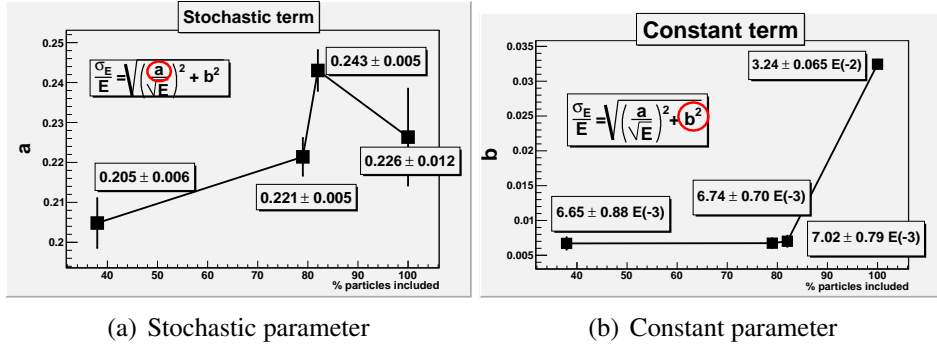
(a) Stochastic parameter (b) Constant parameter

Figure 7: σ_E/E values for different cuts. The x-axis is the percentage of particles remaining after the cut is performed. The most number of particles remain for the "strict" cut, and the least for the "sector" cut.

parameters a and b for the gapless model are comparable to the parameter values plotted in figure 7, which were derived by cutting out particles in post-processing. This is a good check that excluding tile gap particles approaches the behavior of a calorimeter with no tile gaps.

The second salient attribute, seen clearly in figures 5(b), 5(c), and 5(d), is that the energy deposition within the gap is smeared, instead of being a clear second distribution separate from that of particles incident on the sensored regions. The tradeoff to improved energy resolution with a strict cut is that 18% of the total particles were excluded. A similar strategy implemented at the ILC will result in either poorer statistics or will require a longer running time. Attempts to reconstruct azimuthal angle for incident particles and apply a separate correction factor for tile gaps are currently under investigation. Further work will help determine which effect will have a greater impact on energy resolution, the loss of 18% of the particles or the greater energy deposition RMS of tile-gap particles, or if LumiCal configurations are better able to compensate for the tile gaps.
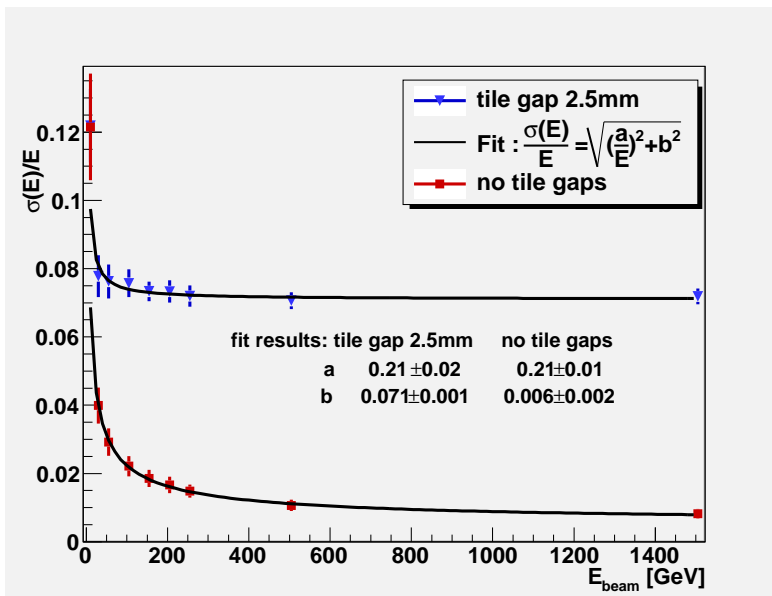
Figure 8: Effect of tile gaps on energy resolution, in particular the leakage parameter b.

References

[1] Geant4: a toolkit for the simulation of the passage of particles through matter. http://geant4.web.cern.ch/geant4/.

[2] International Detector Advisory Group. http://www.linearcollider.org/physics-detectors/Detectors/IDAG.

[3] LHEP physics list. http://www.slac.stanford.edu/comp/physics/geant4/slac_physics_lists/ilc/LHEPlistdoc.html.

[4] Mokka. http://polzope.in2p3.fr:8081/MOKKA/.

[5] H. Abramowicz. Luminosity measurement. ALCPG and ILC Workshops 2005, Snowmass, Colorado, USA.

[6] Ties Behnke, Chris Damerell, John Jaros, and Akiya Miyamoto, editors. *International Linear Collider Reference Design Report, Volume 4: Detectors*, volume 4. ILC Global Design Effort and World Wide Study, 2007. http://www.linearcollider.org/about/Publications/Reference-Design-Report.

[7] James Brau, Yasuhiro Okada, and Nicholas Walker, editors. *International Linear Collider Reference Design Report, Volume 1: Executive Summary*. 2007. http://www.linearcollider.org/about/Publications/Reference-Design-Report.

[8] H. Abramowicz et. al. Monte carlo study of a luminosity detector for the international linear collider, 2005.

[9] W. Wierba et al. Lumical mechanical design proposal and integration with ild. EUDET-Memo-2008-13. http://www.eudet.org/e26/e28.

[10] W. Wierba et al. Lumical new mechanical structure. EUDET-Memo-2009-10. http://www.eudet.org/e26/e28.

[11] W. Wierba et al. Lumical design overview. In *Proceedings of the Workshop of the Collaboration on Forward Calorimetry at ILC*, Vinča Institute of Nuclear Sciences, September 2008. http://www.vinca.rs/pub/FCAL_Belgrade.pdf.

[12] Christian W. Fabjan and Fabiola Gianotti. Calorimetry for particle physics. *Review of Modern Physics*, 75(4):1243–1286, October 2003.

[13] Iftach Sadeh. Luminosity measurement at the International Linear Collider. Master's thesis, Tel Aviv University School of Physics and Astronomy, 2008.

[14] Achim Stahl. Luminosity measurement via bhabha scattering: Precision requirements for the luminosity calorimeter. LC-DET-2005-004 (2005).